Available online at www.sciencedirect.com
SCIENCE DIRECT®
Advances in Water Resources 28 (2005) 1010–1020
Advances in Water Resources
www.elsevier.com/locate/advwatres

Sorptivity and liquid infiltration into dry soil

Patricia J. Culligan [a,*], Vladimir Ivanov [b], John T. Germaine [b]

[a] Department of Civil Engineering and Engineering Mechanics, Columbia University, 610 S.W. Mudd Building, 500 West 120th Street, New York, NY 10027, USA
[b] Department of Civil and Environmental Engineering, Massachusetts Institute of Technology, Cambridge, MA 02139, USA

Received 2 April 2004; received in revised form 13 April 2005; accepted 14 April 2005
Available online 29 June 2005

Abstract

The sorptivity S quantifies the effect of capillarity on liquid movement in a porous material. For liquid infiltration into an initially dry material, S is a parameter that is contingent on both liquid and material properties as well as the maximum liquid content behind the infiltrating front, θ_m. Scaling analyses are used to derive a dimensionless, intrinsic sorptivity S^* that is constant for different liquids, Miller-similar materials and different values of θ_m. The analyses confirm that S is dependent on $\beta^{1/2}$, where $\beta = \cos\phi$ is a measure of the wettability of the liquid. They also indicate a power law relationship between S and $S_{e(av)}$, the average liquid saturation behind the infiltrating front. Seventeen water and eleven Soltrol 220 horizontal infiltration experiments are reported in uniform, dry sand. Test results show that water is partially wetting in the sand. They also confirm that $S \propto S_{e(av)}^d$, where $d = 3.2$ for the experimental conditions. The usefulness of a general, dimensionless Boltzmann variable is demonstrated to normalize infiltration profiles for the different liquids. An approximate method for sorptivity calculation is shown to provide an accurate estimate of S^*.

Keywords: Unsaturated flow; Contact angle; Wettability; Miller scaling

1. Introduction

The process by which a wetting liquid displaces air in a porous material, usually termed liquid infiltration, has been the subject of study for over a century [1–8]. In soils, understanding liquid infiltration in dry or partially saturated media is important for forecasting moisture distribution following soil irrigation [9], estimating the potential for water flux through a landfill cover [10] and predicting a contaminant's transport to groundwater following a surface spill [11]. In porous building materials, such as concrete and masonry, knowledge of liquid infiltration is important for assessing a material's durability and appearance [12]. Many models have been developed to describe liquid infiltration in a porous material, including those by Parlange and co-workers [6,13–19]. These models predict the time-rate of infiltration and the cumulative volume of infiltration based on parameters like the sorptivity S [20], which quantifies the effect of capillarity on a liquid's movement in a material.

The effect of capillarity on liquid movement in an unsaturated material can be isolated by considering horizontal flow, where gravitational forces in the direction of the movement can be neglected. Horizontal one-dimensional flow of a liquid in a rigid, stationary porous material may be described by a non-linear diffusion equation, often referred to as Richard's equation [20]

$$\frac{\partial\theta}{\partial t} = \frac{\partial}{\partial x}\left(D(\theta)\frac{\partial\theta}{\partial x}\right), \tag{1}$$

where θ is the average volumetric liquid content of the infiltrating fluid, $D(\theta)$ is the hydraulic diffusivity, t is the time and x the spatial coordinate.

The hydraulic diffusivity is a non-linear function of liquid content given by

* Corresponding author. Tel.: +1 212 854 3154; fax: +1 212 854 6267.
E-mail address: culligan@civil.columbia.edu (P.J. Culligan).

0309-1708/$ - see front matter © 2005 Elsevier Ltd. All rights reserved.
doi:10.1016/j.advwatres.2005.04.003

$$D(\theta) = K(\theta)\frac{\partial h}{\partial \theta}, \tag{2}$$

where K is the hydraulic conductivity of the material at liquid content θ and h is the liquid pressure head at the same liquid content. The magnitude of h will depend upon the curvature of the liquid–air meniscus, which will be a function of a medium's pore space geometry as well as θ. Idealized models of pore space geometry are usually adopted for media whose pore space are irregular and complex, and cannot be described analytically. A common approach is to use a capillary tube model in which h is estimated using the Young–Laplace equation for a cylindrical tube [21] written in terms of the pressure head. The capillary tube model idealizes the curved liquid–air meniscus within a pore space of average radius r, as a spherical liquid–air meniscus within a capillary tube of the same radius. If the air at the liquid–air meniscus is at atmospheric pressure, then

$$h \approx -\frac{2\sigma\cos\phi}{r\rho g} = -\frac{2\sigma\beta}{r\rho g}, \tag{3}$$

where σ is the surface tension of the liquid, ϕ is the average contact angle of the liquid–air interface at the solid surfaces, ρ is the liquid's density, g is the gravitational constant and $\beta = \cos\phi$, a parameter that is referred to as the "wetting index" [22].

Relationships between h and θ, and K and θ are often described by power laws of the form [20]

$$\frac{h_{\text{entry}}}{h(\theta)} = \left(\frac{\theta-\theta_i}{n-\theta_i}\right)^a = S_e^a \tag{4}$$

and

$$K(\theta) = \frac{kk_r\rho g}{\mu} = K_s S_e^b, \tag{5}$$

where h_{entry} is the pressure head in the liquid at air-entry in the medium, θ_i is the irreducible liquid content, n is the porosity of the medium, S_e is the effective liquid saturation, k is the intrinsic permeability of the medium, k_r is the relative permeability, K_s is the saturated hydraulic conductivity, μ is the liquid viscosity and a and b are empirical coefficients. For liquid drainage, it is common to assume that $a = 1/\lambda$ and $b = (3 + 2/\lambda)$, where λ is the Brooks–Corey pore size distribution index [20]. In cases where $\theta_i \approx 0$, $S_e \approx \theta/n$, hence $\theta \approx S_e n$. Note, for liquid infiltration it will be assumed that the initial liquid content in the medium is θ_i. This assumption is reasonable for primary, but not secondary, wetting of a porous material [20].

Combining Eqs. (3) and (4) gives $r(\theta) = r_{\text{entry}}S_e^a$, where r_{entry} is the average radius of the pores where air first enters the medium, and β is assumed constant for a given liquid and material. Hence, r will vary with S_e, assuming r_{entry} depends only on pore space geometry and β. From Eq. (5) it is clear that k_r also varies with S_e.

To obtain Eq. (1) in the form of an ordinary differential equation, the Boltzmann transformation, $\Phi = xt^{-1/2}$ is used, leading to the solution

$$x(\theta, t) = \Phi(\theta)t^{1/2}, \tag{6}$$

for the boundary conditions $\theta = \theta_i$ at $\Phi = \infty$ and $\theta = \theta_m$ at $\Phi = 0$. These boundary conditions were satisfied for the experiments reported here.

For liquid infiltration into a porous material that is initially dry (i.e, $\theta_i = 0$), the volume of liquid infiltration per unit area is therefore

$$i(t) = t^{1/2}\int_0^{\theta_m} \Phi\, d\theta. \tag{7}$$

By definition $\int_0^{\theta_m}\Phi\, d\theta$ is the sorptivity S of the material [23]. S can be determined from observations of liquid infiltration with time into a porous material [18]. S is related to $D(\theta)$ by

$$S = -2D(\theta_m)\frac{d\theta_m}{d\Phi}. \tag{8}$$

Hence

$$S = -2K(\theta_m)\frac{dh_m}{d(x/t^{1/2})}. \tag{9}$$

For an initially dry soil, S is a function of the properties of the porous material, including its grain size distribution and packing, the properties of the infiltrating liquid and θ_m. An intrinsic sorptivity, S^*, that is independent of these variables, can be defined for geometrically similar materials by applying the principles of Miller-scaling [24] to Eq. (9), viz.

$$S = \left(\frac{l\beta\sigma\theta_m}{\mu S_{e_m}^c}\right)^{1/2} S^*, \tag{10}$$

where the following scaling relationships have been used [25,26]

$$h^* = \frac{lS_{e_m}^a\rho g}{\sigma\beta}h, \tag{11}$$

$$K^*(\theta_m) = \frac{\mu}{l^2 S_{e_m}^b\rho g}K(\theta_m), \tag{12}$$

$$d^*(\,) = Ld(\,), \tag{13}$$

$$x^* = \frac{x}{L}, \tag{14}$$

$$t^* = \frac{\sigma\beta l S_{e_m}^b}{\mu L^2\theta_m S_{e_m}^a}t, \tag{15}$$

where the superscript $*$ denotes a dimensionless variable, μ is a characteristic microscopic length of the material, L is a macroscopic length and $c = a - b$. $S_{e(m)}$ is the value of S_e at $\theta = \theta_m$. Note, ρg and $S_{e(m)}$ are sometimes omitted from Eqs. (11) and (12), e.g., [25]. These terms have been included to establish non-dimensional variables and account for the fact that r and k_r are functions

of S_e [20]. It has been assumed that $r = lS_e^a, k = l^2$ and $k_r = S_e^b$.

The intrinsic sorptivity defined by Eq. (10) is more general than alternative definitions provided in the literature [26,27]. Most notably, $S^*$is dimensionless and theoretically applicable to Miller-similar media as well as different values of θ_m. A general, dimensionless Boltzmann variable can also be derived from Eqs. (14) and (15), namely

$$\Phi = \left(\frac{\sigma\beta l}{\mu\theta_m S_{e_m}^c}\right)^{1/2} \Phi^*. \tag{16}$$

Profiles of Φ^* versus $\theta^*(x,t)$ should match for Miller-similar materials, where

$$\theta^*(x,t) = \frac{\theta(x,t) - \theta_i}{\theta_m - \theta_i}. \tag{17}$$

θ_m may be less than n due to entrapment of air in pores or liquid bypassing of pores during the infiltration process [19]. Quantifying θ_m usually requires destructive sampling of a porous material following an infiltration test [20]. It is, however, straightforward to establish the average liquid content behind an infiltrating front during an infiltration test from $\theta_{av} = i(t)/x(t)$. In what follows it will be assumed that replacing θ_m with θ_{av} and $S_{e(m)}$ with $S_{e(av)}$ in the scaling laws presented above does not invalidate the relationships.[1] Because $\theta_{av} < \theta_m$, values of S^* and Φ^* based on θ_{av} and $S_{e(av)}$ will be higher than those based on θ_m and $S_{e(m)}$.

Re-writing Eq. (10) in terms of θ_{av} and $S_{e(av)}$, and making use of the fact that $\theta_{av} = S_{e(av)}n$ for infiltration into an initially dry material where $\theta_i = 0$, gives

$$S = \left(\frac{l\beta\sigma n}{\mu S_{e_{av}}^{(c-1)}}\right)^{1/2} S_{av}^*. \tag{18}$$

Hence, for liquid infiltration into dry material $S \propto S_{e(av)}^{-(c-1)/2}$ for a given material and liquid pair. Note, the subscript (av) is used to clarify that a dimensionless variable has been defined using θ_{av} and $S_{e(av)}$.

For water (subscript w) and an organic liquid (subscript o) infiltrating into the same material at the same $S_{e(av)}$, Eq. (18) predicts that $S_w/S_o = (\beta_w\sigma_w\mu_o/\beta_o\sigma_o\mu_w)$. Research on the scaling of capillary behavior for air–water and air–organic liquid systems in coarse soils (i.e., sands) has concluded that $(\beta_w/\beta_o) = 1$ [28,29], suggesting that $S_w/S_o = (\sigma_w\mu_o/\sigma_o\mu_w)$ for liquid infiltration into dry sand if n is held constant and $S_{e(av)}$ is homologous.

The work described in this paper was motivated by prior observations made during experiments that examined both the stable and unstable vertical infiltration of either water or Soltrol 220 into uniform dry sand of the same porosity [30,31]. Specifically, data gathered during those experiments provided a mean ratio of $S_w/S_o = 2.4$, which is approximately 70% of that predicted by $S_w/S_o = (\sigma_w\mu_o/\sigma_o\mu_w)$. To investigate why the observed ratio S_w/S_o was lower than expected, including the significance of β and S_e, a series of water and Soltrol 220 horizontal infiltration experiments was conducted into a uniform, dry soil packed at an average porosity $n = 0.38$. The choice of horizontal liquid infiltration reduced the impact of gravitational forces. The use of an initially dry, uniform material eliminated liquid bypass/cut-off as an important infiltration mechanism [32,33]. $S_{e(av)}$ was varied by changing the liquid pressure head, h_0, at the inlet to the porous medium. In what follows, the liquids and the material used in the experiments are described, together with the experimental apparatus and the experimental procedures. The results of the experiments are then presented and their interpretation is discussed.

2. Materials and experimental procedures

2.1. Liquids and porous medium

Two liquids were used for the infiltration experiments, namely distilled water and Soltrol 220, an aliphatic oil purchased from Philips 66, Inc. Properties of these liquids are given in Table 1.

All liquid infiltration experiments were conducted using a quartz sand purchased from WHIBCO Inc., New Jersey, with an average grain diameter of 0.15 mm and a uniformity coefficient $C_u = D_{60}/D_{10} = 1.9$. The sand, which is referred to as New Jersey Fine Sand (*NJFS*), was passed through ASTM Sieve #30 (metric equivalent 600 μm) and the retained portion was removed. To prevent accidental contamination or moistening, the sand was stored in a sealed plastic bucket. Fig. 1 presents the soil moisture characteristic (SMC) curve of the sand. The SMC was obtained using a continuous drying technique developed at the Massachusetts Institute of Technology (MIT) [34]. The moisture evaporation rate from the sand during the drying was approximately 12.5 g/day. Table 2 summarizes the

Table 1
Properties of Soltrol 220 and water at 20 °C

Property	Soltrol 220[a]	Water
Dynamic viscosity, μ (g/cm/s)	4.12×10^{-2}	1.002×10^{-2}
Density, ρ (g/cm^3)	0.795	0.998
Surface tension, σ (dyne/cm)	25.3	71.9

[a] Properties for Soltrol 220 were obtained from manufacturer's tables.

[1] For infiltration processes that are well described by the Green–Ampt model [2] this assumption will be reasonable because, by definition, the Green–Ampt model assumes that $\theta_m = \theta_{av}$.

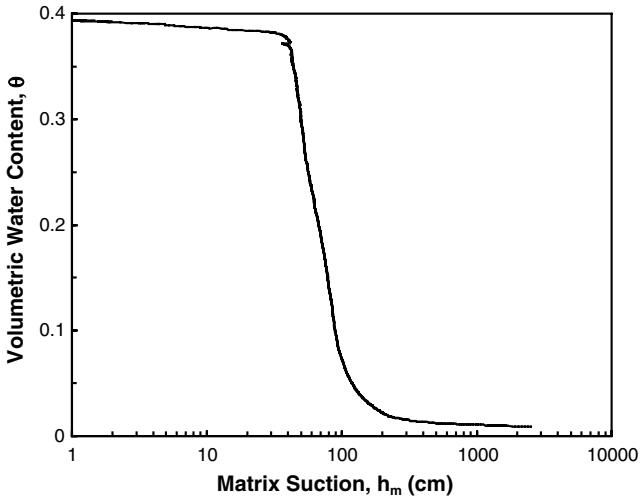

Fig. 1. Soil moisture characteristic curve of the sand during drying. The sand was packed at a porosity $n = 0.4$ and fully saturated using de-aired pure water at high pressure before drying commenced. θ is the volumetric water content of the sand and h_m is the measured metric suction in cm of water.

Table 2
Properties of New Jersey Fine Sand (NJFS)

Property	
Average particle size, D_{50} (cm)	0.015
Saturated conductivity, water $K_{s(w)}$ (cm/s)[a]	6.7×10^{-3}
Saturated conductivity, Soltrol 220 $K_{s(o)}$ (cm/s)[a]	1.3×10^{-3}
Air-entry pressure, h_{entry} (cm water)[b]	−40
Irreducible volumetric water content during drying, θ_i[b]	0.009
Brooks–Corey λ[b]	2.2

[a] From constant head test (ASTM 2434-68).
[b] From soil–moisture characteristic curve (see Fig. 1).

properties of the sand. The pore distribution index λ was obtained by fitting the Brooks–Corey relationship [20] to the SMC curve. Because λ was obtained from a drying curve, it might not be an accurate representation of the pore distribution index for wetting.

2.2. Experimental apparatus

A schematic of the apparatus used for the horizontal infiltration experiments is shown in Fig. 2. The apparatus is similar to that used in prior research that examined the applicability of moisture diffusion theories for predicting liquid infiltration in soil [4]. Here, the sand was placed in a transparent tube whose cross-sectional area was either circular with an internal diameter of 2.54 cm, or square (either a closed or open channel) with internal dimensions of 2.25×2.25 cm. The maximum vertical height of a tube, h_{tube}, was at least an order of magnitude less than the maximum value initially estimated for h using Eq. (3).[2] Hence, gravitational effects due to the variation of h_0 with vertical position in a tube were assumed to be negligible.

The tubes, which were either 70 cm or 40 cm in length, were annotated by measuring tape marked in 1 mm divisions. The inlet port to a tube consisted of a 3-valve chamber with a brass mesh screen and filter paper system that allowed liquid to enter the tube but prevented sand loss. The opening size of the mesh screen was 0.35 mm, which is greater than the D_{50} of the sand. Both the mesh screen and filter paper were wetted with the liquid infiltrant prior to an experiment. A soft tubing line, attached to the inlet valve, connected the chamber to the infiltrant container. The infiltrant container rested on a scale that was used to record the cumulative mass of liquid infiltration into the tube with time. A second container was connected by soft tubing to a base valve in the inlet chamber. This container was used for the initial flooding and final drainage of the chamber. A cap with an opening to atmosphere held the soil in place at the end of each tube while permitting free air drainage. Thus, air was free to escape during all experimental configurations.

Sand was uniformly deposited into the tubes using a multiple sieve pluviation technique described by Ivanov [35]. This technique resulted in sand specimen with dry bulk densities in the range of 1.63–1.69 g/cm^3, and porosities in the range of 0.37–0.39. The sieve analyses of sand samples taken from the storage bucket and the dry portion of a tube (between the terminal position of the wetting front and the end cap, Fig. 2) after an infiltration experiment, confirmed that the grain size distribution of the sand remained consistent throughout the experimental program.

2.3. Experimental procedure

After the sand was pluviated into the tube, the apparatus was assembled and positioned so that it was approximately horizontal. The infiltrant container was then filled with liquid and placed on the electronic balance. The inlet tube, flexible inlet line and inlet valve were saturated with the liquid, then the inlet valve was closed and attached to the inlet chamber. Next, liquid was placed in the flooding containers, and the flexible flooding line and the flooding valve were saturated. The flooding valve was closed and attached to the inlet container. The infiltrant container was then moved relative to the horizontal tube in order to set the desired inlet pressure head, h_0. The tube was leveled horizontally and secured. The top air valve and the flooding valve were opened and the inlet chamber was saturated with liquid. The electronic scale was zeroed. An instant later,

[2] h was initially estimated taking $\cos\theta = 1$ and $r = 0.004$ cm, which is approximately half the D_{10} of the soil.

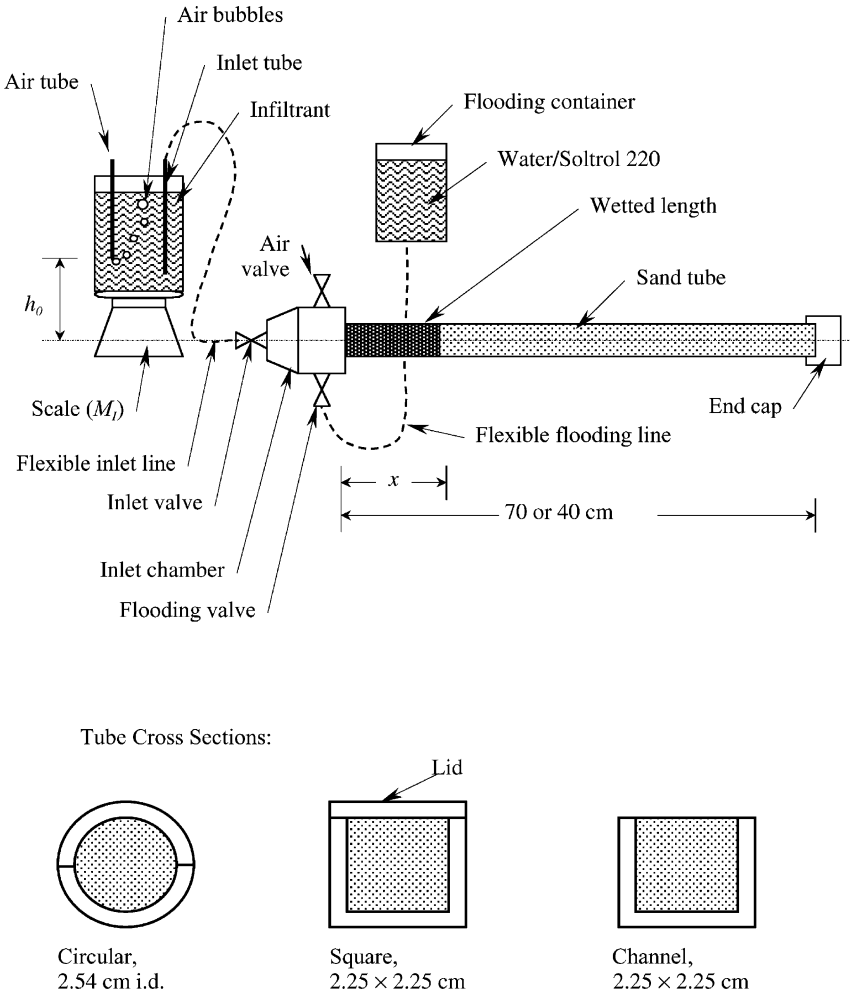

Fig. 2. Schematic diagram of experimental apparatus.

the air and flooding valves were closed, the inlet valve was opened and the clock was started.

During an experiment, the elapsed time, t, the average front position $x(t)$, and the cumulative infiltration by mass M_I, were recorded. The average front position was read to an accuracy of about 1 mm from the annotated measuring tape. All experiments were conducted at an ambient temperature of approximately 20 °C.

Before the liquid front wetted 90% of the tube, the flooding container was lowered and the inlet valve was closed. Both the air and the flooding valves were then opened to drain the chamber and terminate the experiment. Depending upon the liquid and the applied inlet pressure head, the duration of the experiments ranged between 40 min and 8 h.

During each experiment, the nature of the flow was closely observed in search of evidence of fingering, pockets of dry soil behind the wetting front, separation of the sand from the tube walls, and/or an abrupt decrease of the advance rate, all of which might indicate the presence of loose sections of sand. None of the data presented here were affected.

Final liquid distributions were obtained at the end of a sub-set of experiments conducted at $h_0 = 0$. Fig. 3 illustrates the employed sampling technique. A set of thin brass pieces (knives), matching the shape of the tube cross-section, was inserted into the sand to partition the tube into sections. Giving preference to sampling closely behind the front, specimen, with dry masses between 2 and 15 g, were acquired. The wet mass of the specimens were determined and then oven dried to enable calculation of the gravimetric liquid content, w. Before oven drying, the samples containing Soltrol 220 were first soaked and then washed with a solution of distilled water and Alconox®, an anionic detergent, before a final rinse with distilled water. In order to limit the sand particle loss, the soaking and rinsing of the Soltrol 220 samples was conducted only once. The gravimetric liquid content was converted to the volumetric liquid content using:

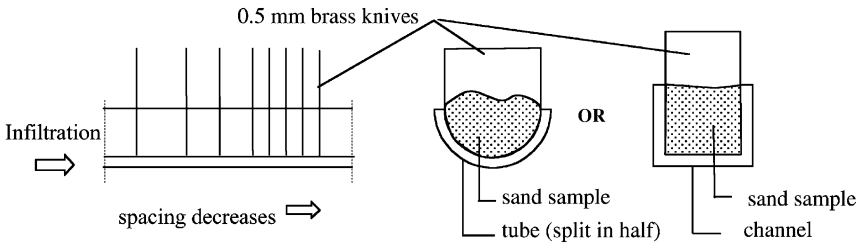

Fig. 3. Sampling for liquid content measurements at the end of an experiment.

$$\theta = w\frac{\rho_b}{\rho}, \tag{19}$$

where w and ρ_b denote the gravimetric liquid content and the average dry density of the sand column, respectively.

2.4. Interpretation of experimental data

The cumulative infiltration of liquid per unit area, $i(t)$ was obtained from

$$i(t) = \frac{M_I(t)}{A\rho}, \tag{20}$$

where A is the cross-sectional area of the tube.

The value of S for each experiment was obtained from a linear regression of $i(t)$ versus $t^{1/2}$. As shown in Fig. 4, $i(t)$ and $x(t)$ are linear with $t^{1/2}$.

As noted in the introduction, the average volumetric liquid content of the wetted material in the tube was estimated from

$$\theta_{av}(t) = \frac{i(t)}{x(t)}. \tag{21}$$

The average effective saturation was calculated from $S_{e(av)} = \theta_{av}/n$, where θ_{av} was taken as $\theta_{av}(t)$ at the end of an experiment.

A total of 28 horizontal infiltration tests were performed: 17 using water as the infiltrating liquid (*NW* series) and eleven using Soltrol 220 (*NL* series). The range of h_0 was −30 cm to +50 cm of liquid, giving rise to $S_{e(av)}$ values between 0.45 and 0.85.

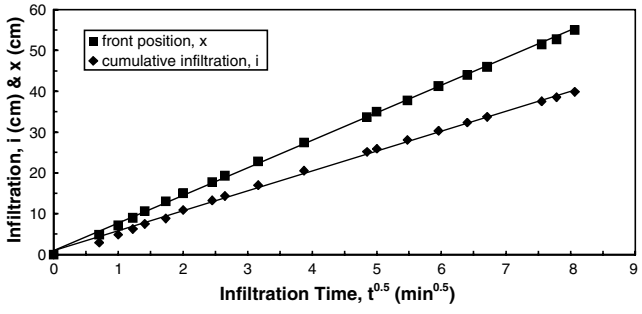

Fig. 4. Plot of $i(t)$ versus $t^{1/2}$ for *NW8*, an experiment conducted using water as the infiltrating fluid in a circular tube. The inlet head $h_0 = +5$ cm. The linear relationship between $x(t)$ and $t^{1/2}$ is also displayed.

3. Discussion of results

Table 3 presents a summary of results for the water infiltration experiments, while Table 4 summarizes results for the Soltrol 220 experiments.

Fig. 5 displays $\theta_{av}(t)$ versus $x(t)$ for select experiments conducted with water as the infiltrant. $\theta_{av}(t)$ was constant over much of the infiltration process and less than n. Theoretically, $\theta_{av}(t)$ should have reached an asymptote after a few millimeters, when local variations in r no longer influenced the average front position. However, the experimental data indicate that it took a few centimeters for $\theta_{av}(t)$ to stabilize. This inconsistency is put down to the difficulty of zeroing the scale used to record M_I at exactly the time when $x = 0$. As seen in Fig. 4, zeroing of the scale slightly lagged liquid infiltration, leading to under-estimation of θ_{av} at early times. With increasing time this error became insignificant. Fig. 5 shows that the asymptotic value of $\theta_{av}(t)$, and hence $S_{e(av)}$, increased with increasing h_0. The trends displayed in Fig. 5 were also observed for the experiments were Soltrol 220 was the infiltrant.

The observed relationships between S and the inlet head, h_0 is shown in Fig. 6. S increases with h_0 because $S_{e(av)}$ increases with h_0. The tube's shape had no apparent influence on the experimental results, leading to the conclusion that an open tube, the easiest cross-section to work with, is a good choice for future experiments provided that the influent level stays below the soil surface, i.e., provided that $h_0 \leqslant h_{tube}/2$. Note, this would limit h_0 to about 1 cm for the channel used in the experiments reported here. The open channel also lends itself to soil surface instrumentation that might enable the simultaneous measurement of liquid pressures during infiltration.

The relationships between S and h_0 are well described empirically by second order functions, as shown in Fig. 6. These functions provide an estimate

$$\left.\frac{S_w}{S_o}\right|_{h_0=0} = \frac{0.207}{0.085} = 2.4. \tag{22}$$

Table 3
Summary of water infiltration experiments

Experiment no.	Porosity n	Tube cross-section	h_0 (cm)	θ_{av}	$S_{e(av)}$	S (cm/s$^{1/2}$)
NW13	0.37	Circular	−30	0.16	0.44	0.038
NW11	0.38	Circular	−15	0.27	0.71	0.127
NW5	0.37	Circular	−10	0.27	0.74	0.170
NW6	0.38	Circular	−10	0.25	0.66	0.160
NW12	0.37	Circular	−5	0.27	0.73	0.189
NW1	0.36	Circular	0	0.23	0.64	0.176
NW15	0.37	Circular	0	0.26	0.7	0.187
NW2	0.37	Circular	0	0.26	0.7	0.201
NW7	0.37	Circular	0	0.29	0.77	0.227
NW16	0.39	Square	0	0.27	0.69	0.192
NW17	0.39	Channel	1.12	0.29	0.75	0.234
NW8	0.39	Circular	5	0.28	0.73	0.249
NW3	0.37	Circular	10	0.27	0.73	0.242
NW4	0.38	Circular	10	0.28	0.73	0.256
NW9	0.37	Circular	15	0.29	0.78	0.271
NW10	0.38	Circular	15	0.29	0.75	0.280
NW14	0.37	Circular	50	0.31	0.85	0.411

Table 4
Summary of Soltrol 220 infiltration experiments

Experiment No.	Porosity n	Tube cross-section	h_0 (cm)	θ_{av}	$S_{e(av)}$	S (cm/s$^{1/2}$)
NL 6	0.36	Circular	−10	0.23	0.64	0.051
NL 7	0.37	Circular	−10	0.26	0.7	0.053
NL 1	0.37	Circular	0	0.24	0.66	0.078
NL 2	0.37	Circular	0	0.28	0.75	0.089
NL 3	0.37	Circular	0	0.27	0.73	0.088
NL 10	0.39	Square	0	0.32	0.82	0.098
NL 11	0.39	Circular	0	0.34	0.86	0.097
NL 9	0.39	Channel	3	0.32	0.82	0.11
NL 4	0.37	Circular	10	0.26	0.71	0.099
NL 5	0.36	Circular	10	0.23	0.63	0.083
NL 8	0.38	Circular	50	0.32	0.84	0.184

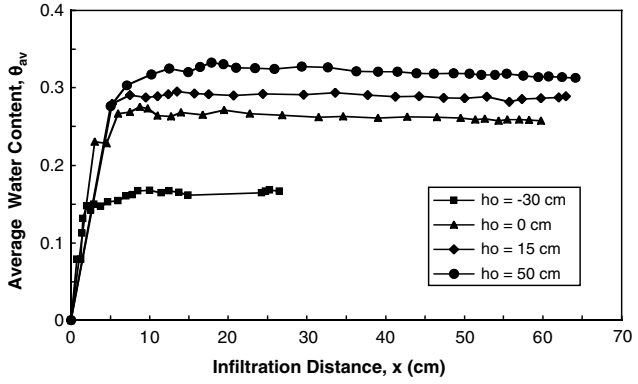

Fig. 5. $\theta_{av}(t)$ versus $x(t)$ for select water infiltration experiments.

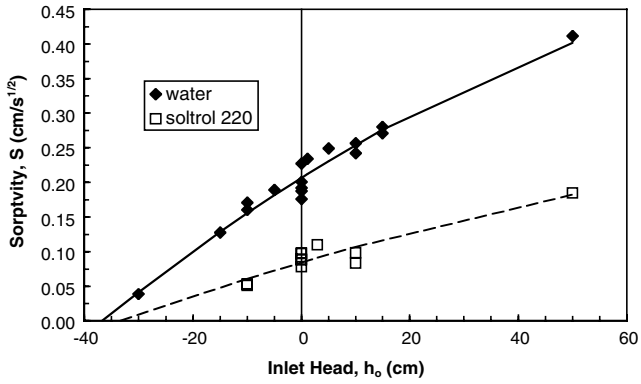

Fig. 6. Observed relationships between S and h_0. The symbols are experimental data. The lines are empirical relationships between S and h_0 that assume a second order polynomial. The fitted relationship for the water (solid line) is; $S_w = -2 \times 10^{-5} h_0^2 + 0.0049 h_0 + 0.207$; $R^2 = 0.97$, while that for the Soltrol 220 (dashed line) is $S_o = -7 \times 10^{-5} h_0^2 + 0.0023 h_0 + 0.0845$; $R^2 = 0.88$.

Hence, the observed ratio for S_w/S_o was the same as the previous result [30,31].

Fig. 7 illustrates the observed correlations between S and $S_{e(av)}$. A plot of $\log_{10}(S)$ versus $\log_{10}(S_{e(av)})$ is given in Fig. 8. A theoretical power law of the form $S = AS_{e(av)}^d$ is included on both figures, where

$$A = \left(\frac{l\beta\sigma n}{\mu}\right)^{1/2} S^* \tag{23}$$

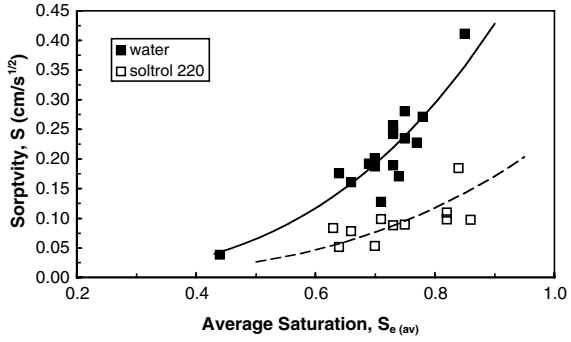

Fig. 7. Observed relationships between S and $S_{e(av)}$. The solid line is the power law $S = 0.6S_{e(av)}^{3.2}$. The dashed line is the power law $S = 0.24S_{e(av)}^{3.2}$.

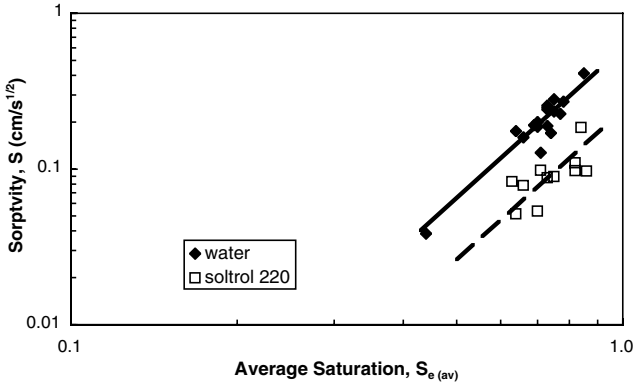

Fig. 8. $\mathrm{Log}_{10}(S)$ versus $\log_{10}(S_{e(av)})$. The solid line is the power law $S = 0.6S_{e(av)}^{3.2}$. The dashed line is the power law $S = 0.24S_{e(av)}^{3.2}$.

and

$$d = -\left(\frac{c-1}{2}\right). \tag{24}$$

Note, to obtain the correlations, the value of d was constrained to be the same for the water and the Soltrol 220 results.

The data displayed in Figs. 7 and 8 show some scatter. Nonetheless, the relationships between S and $S_{e(av)}$ appear to be well described by the power laws. The ratio $A_w/A_o = 2.5$. Thus, from Eq. (23) $\beta_w/\beta_o = 0.53$, assuming no significant variation of l and n between experiments. The value of d is 3.2. Hence $c = -5.4$. The Brooks–Corey relationship for soil drainage forecasts a lower c of -3.45, suggesting less variation in S with $S_{e(av)}$ than was observed. The difference between the observed and estimated values of c might be explained by the fact that c was estimated using a λ value that was obtained from a drying, rather than a wetting, curve. Steffy et al. [36] report a systematic study of drying and wetting curves for air–water and air–organic fluid pairs in sand with properties similar to *NJFS*. The results of Steffy et al. support the observation that λ values estimated from drying curves are higher, and hence c values are lower, than those estimated from wetting curves.

Another estimate of the ratio β_w/β_o can be acquired by considering the ratio h_w/h_o, which from Eq. (3) is $\left(\frac{\sigma_w\rho_o}{\sigma_o\rho_w}\right)\beta_w/\beta_o$ if $r_w = r_o$. The pressure head at the infiltrating front was not measured during the experiments. However, an estimation of h when $S = 0$ can be obtained from the empirical relationships provided in Fig. 6; namely, $h_{w,S=0} = -37$ cm and $h_{o,S=0} = -33$ cm . When $S = 0$ liquid is not advancing in the medium. Thus, the liquid–air interface is under static-equilibrium [37]. The radius of curvature of a static liquid–air interface is determined by the pore geometry of a material. Hence, it is reasonable to assume that $r_w = r_o$ at $S = 0$, leading to an estimate of $\beta_w/\beta_o = 0.50$, which is close to the value obtained from Eq. (23) and confirms that $\beta_w < \beta_o$.

Taylor et al. [26] also reported $\beta_w < \beta_o$ in experiments that examined organic liquid and water adsorption into dry calcite limestones. Taylor et al. concluded that the organic liquids completely wet the limestones, hence $\beta_o = 1$. Partial water wetting in the limestones, which resulted in $\beta_w < 1$, was attributed to organic adlayers that rock mineral surfaces acquire when exposed to the natural environment. Work by Bromwell [38] has shown that the mineral surfaces of quartz sands are often contaminated with oil that is hard to remove even with repeated chemical cleaning. Oil contamination of mineral surfaces is therefore put forward as a reason for $\beta_w < 1$ in the experiments reported here. $\beta_w < 1$ would also explain the "low" S_w/S_o ratio observed in the prior experiments [30,31].

To quantify the dimensionless sorptivity from Eq. (23), the Soltrol 220 is assumed to completely wet the *NJFS*, giving $\beta_o = 1$ and $\beta_w = 0.53$. Adopting a value $l = D_{50}$ (see Table 2) and assuming a characteristic porosity $n = 0.38$ (see Tables 3 and 4) gives $S^*_{av} = 0.128$.

Fig. 9 provides a plot of $\theta(x, t_{end})$ versus Φ for selected water and Soltrol 220 experiments conducted at $h_0 = 0$, where t_{end} is the time at the end of the experiment when liquid content as a function of x was determined.

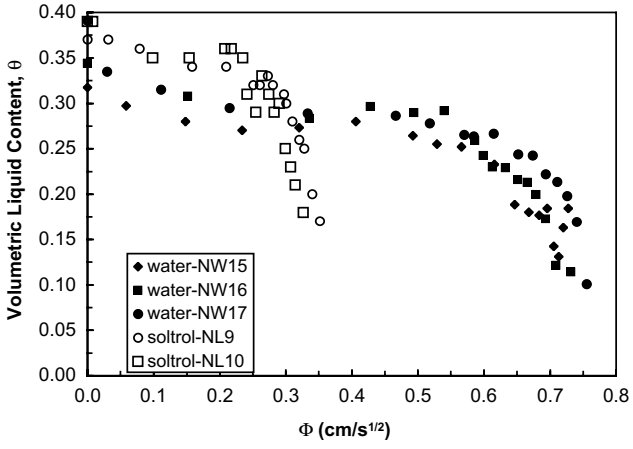

Fig. 9. $\theta^*(x, t_{end})$ versus Φ.

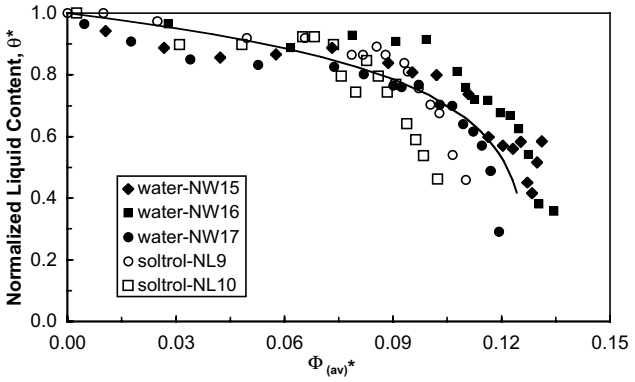

Fig. 10. $\theta^*(x, t_{end})$ versus Φ^*_{av}. The solid line is the approximation provided by Eq. (26) using $m = 6$ and $s^*_{av} = 0.105$.

The data show some scatter, leading to the conclusion that a better sampling technique for θ is needed. The knives shown in Fig. 3 were inserted in a sequence that moved backward from the wetting front to the tube inlet. This caused liquid redistribution in sand that resulted in liquid being squeezed back to the inlet. Hence, the measured liquid content at the inlet might be higher than θ_m. As expected, the profiles for water and the Soltrol 220 experiments are distinct. Fig. 10 is a plot of $\theta^*(x, t_{end})$ versus Φ^*_{av} for the same data. $\theta^*(x, t_{end})$ was obtained from Eq. (17) using $\theta_i = 0$ and observed values of θ_m. Φ^*_{av} was calculated using $\beta_o = 1$, $\beta_w = 0.53$, $l = D_{50}$ and $c = -5.4$ (see Fig. 7). Excepting the scatter, the profiles of $\theta^*(x, t_{end})$ versus Φ^*_{av} are approximately equivalent for the water and the Soltrol 220, indicating that the generalized dimensionless Boltzmann variable provides the correct scaling, even when it is defined using θ_{av} and $S_{e(av)}$ instead of θ_m and $S_{e(m)}$.

An approximation provided by Parlange and co-workers [19] can be used to estimate the dimensionless sorptivity S^*_{av} from the similarity profile given in Fig. 10. Taking the dependence of the diffusivity on θ^* to be exponential, such that

$$D(\theta^*) = D_0 e^{m\theta^*}, \tag{25}$$

the normalized wetting profile is given by [19]

$$\theta^*(x) \approx \frac{1}{m} \ln\left[e^m - \frac{m}{D^*_0}\left(\frac{s^*}{2}\Phi^* + \beta\Phi^{*2}\right)\right], \tag{26}$$

where

$$D^*_0 = \frac{m^2 (s^*)^2}{e^n(2m-1) - m + 1} \tag{27}$$

and

$$\beta = \frac{1}{2}\left(\frac{1 + m - e^m}{2m(e^m - 1)}\right), \tag{28}$$

where s^* is the *reduced* dimensionless sorptivity and D^*_0 is the dimensionless "constant" diffusivity. It is straightforward to show that $s^*_{av} = (\theta_{av}/\theta_m)S^*_{av}$ and $D^*_{0_{av}} = \frac{\mu S^c_{av}}{l\sigma\beta} D_0$. Note, that the dimensionless "constant" diffusivity changes with the average liquid saturation behind the infiltration front. Thus, it is only a constant for a given $S_{e(av)}$.

Eq. (26) has been fit to the profile given in Fig. 10 using $m = 6$ and $s^*_{av} = 0.105$. The approximate solution is insensitive to m but sensitive to s^* [17]. Therefore, comparative fits using different values of m were found. However, corresponding values of s^*_{av} were observed to remain within 2% of 0.105. The dimensionless constant diffusivity is 9×10^{-5}. Hence, at $h_0 = 0$, $D_0 = 2.3 \times 10^{-3}$ cm^2/s for the water infiltration and $D_0 = 2.0 \times 10^{-3}$ cm^2/s for the Soltrol 220 infiltration.

The average value of θ_{av}/θ_m for the experiments reported in Fig. 10 was 0.79 ± 0.05, leading to an estimated value of $S^*_{av} = 0.133$. This compares well with $S^*_{av} = 0.128$, which was inferred from the results of all infiltration experiments. Thus, the approximation provided by Parlange and co-workers [19] is an accurate way to estimate S^* from an infiltration profile. Knowing S^*_{av}, Eq. (18) can, theoretically, be used to calculate the sorptivity S, for a wide range of conditions.

4. Conclusions

The condition of liquid infiltration into an initially dry material was examined and a dimensionless, intrinsic sorptivity S^* that is independent of material properties, liquid properties and θ_m, the maximum liquid saturation behind the infiltrating front, was derived from scaling analyses. For a given material, the analyses confirm that sorptivity is dependent on $\beta^{1/2}$ [26], where $\beta = \cos\phi$ is a measure of the wettability of the liquid. Upon the assumption that the derived scaling relationships are still valid if θ_m is replaced by the average liquid saturation behind the infiltrating front θ_{av}, the analyses also indicate a power law relationship between sorptivity and the average liquid saturation $S_{e(av)}$. The scaling analyses were also used to derive a dimensionless Boltzmann variable Φ^* that is independent of liquid and material properties. Profiles of normalized liquid content versus Φ^* should match for different liquids and Miller-similar materials.

The dependence of sorptivity on β and $S_{e(av)}$ for infiltration into dry material was investigated in a series of seventeen water and eleven Soltrol 220 horizontal infiltration experiments that were conducted in a uniform, dry sand packed at an average porosity $n = 0.38$. $S_{e(av)}$ was altered by varying h_0, the liquid pressure head at the inlet to the porous medium. h_0 values between -30 cm and $+50$ cm gave rise to $S_{e(av)}$ values between 0.45 and 0.85. The results of the experiments show that

sorptivity $\propto S_{e(av)}^{3.2}$, confirming that a power law relationship between sorptivity and $S_{e(av)}$ is appropriate for porous materials with $\theta_r \approx 0$. The relationship between sorptivity and $S_{e(av)}$ must be known if sorptivity test results are to be used to predict liquid adsorption at saturations that differ from the test's saturation. Experimental results also indicate that $\beta_w/\beta_o = 0.53$. Hence $\beta_w < 1$. This has significant implications for the modeling of unsaturated transport, as it challenges common assumptions that water is fully wetting in coarse soils [28,29]. The observation of partial water wetting is attributed to oil contamination of soil mineral surfaces. Partial water wetting can also explain the "low" S_w/S_o ratio observed in the prior experiments [30,31].

Liquid content profiles for three water and two Soltrol 220 infiltration experiments were used to examine the validity of the dimensionless Boltzmann variable. The liquid content profiles were obtained from destructive sampling of a soil tube at the end of experiment. Excepting the scatter, the profiles of normalized liquid content versus Φ_{av}^* were approximately equivalent, indicating that the dimensionless Boltzmann variable provides the correct scaling for different liquids in the same material, even when it is defined using θ_{av} and $S_{e(av)}$ in place of θ_m and $S_{e(m)}$.

The magnitude of the dimensionless sorptivity, based on θ_{av}, was calculated assuming $\beta_o = 1$, $\beta_w = 0.53$, $l = D_{50}$ and $n = 0.38$, giving rise to $S_{av}^* = 0.128$. An approximate solution provided by Parlange and coworkers [19] provided an accurate estimate of $S_{av}^* = 0.133$. Knowing S_{av}^*, Eq. (18) can, theoretically, be used to calculate the sorptivity S for a broad range of conditions. However, further experiments are required to establish the validity of the scaling analyses for Miller-similar materials. In addition, the assumption that the scaling relationships still hold when θ_m and $S_{e(m)}$ are replaced by θ_{av} and $S_{e(av)}$, should be confirmed for a wider set of experimental conditions.

Acknowledgements

The work was supported, in part, by Dr. Culligan's National Science Foundation career grant CMS-9875883. The authors wish to thank Stephen Rudolph for his assistance in the fabrication of the experimental apparatus. The valuable comments provided by the reviewers of this paper are acknowledged.

References

[1] Slichter CS. Theoretical investigation of the motion of groundwaters. Nineteenth Annual Rep., Pt. 2. Washington DC: US Geological Survey; 1898. p. 295–384.
[2] Green WH, Ampt GA. Studies on soil physics, Part I. Flow of air and water through soils. J Agric Sci 1911;4:1–24.
[3] Green WH, Ampt GA. Studies on soil physics, Part II. Permeability of an ideal soil to air and water. J Agric Sci 1912;5:1–26.
[4] Bruce RR, Klute A. The measurement of soil moisture diffusivity. Soil Sci Soc Am Proc 1956;20:458–62.
[5] Neilson DR, Biggar JW, Davidson JM. Experimental consideration of diffusion analysis in unsaturated flow problems. Soil Sci Soc Am Proc 1962;26:107–11.
[6] Smith RE, Parlange J-Y. A parameter-efficient hydrological infiltration model. Water Resour Res 1978;14(3):533–8.
[7] Babu S, Fox PJ. Model for capillary-induced radial flow in cohesionless soils. Geotech Test J 2000;23(3):369–76.
[8] Ioannou I, Hall C, Wilson MA, Hoff WD, Carter MA. Direct measurement of the wetting front capillary pressure in a clay brick ceramic. J Phys D: Appl Phys 2003;36:3176–82.
[9] Widstoe JA. Dry farming. New York: The Macmillan Co.; 1902.
[10] Vesilind PA, Worell W, Reinhart D. Solid waste engineering. Brooks/Cole; 2002.
[11] Soga K, Kawabata J, Kechavarzi C, Coumoulos H, Waduge WAP. Centrifuge modelling of nonaqueous phase liquid movement and entrapment in unsaturated layered soils. J Geotech Geoenviron Eng, ASCE 2003;129(2):173–82.
[12] Hall C, Hoff WD. Water absorption in brick, stone and concrete. London: Spon Press; 2002.
[13] Hill DE, Parlange J-Y. Wetting front instability in layered soils. Soil Sci Soc Am J 1972;36:697–702.
[14] Parlange J-Y, Lise I, Braddock RD, Smith RE. The three parameter infiltration equation. Soil Sci 1982;133(6):337–41.
[15] Parlange J-Y, Barry DA, Parlange MB, Lockington DA, Haverkamp R. Sorptivity calculation for arbitrary diffusivity. Transport Porous Med 1994;15(3):197–208.
[16] Barry DA, Parlange J-Y, Haverkamp R, Ross PJ. Infiltration under ponded conditions: 4. An explicit predictive infiltration formula. Soil Sci 1995;160:8–17.
[17] Parlange J-Y, Barry DA, Haverkamp R. Explicit infiltration equations and the Lambert-*W*-function. Adv Water Resour 2002;25:1119–24.
[18] Lockington D, Parlange J-Y, Dux P. Sorptivity and the estimation of water penetration into unsaturated concrete. Mater Struct 1999;32:342–7.
[19] Lockington D, Parlange J-Y. Anomalous water absorption in porous materials. J Phys D: Appl Phys 2003;36:760–7.
[20] Tindall JA, Kunkel JR. Unsaturated zone hydrology for scientists and engineers. Englewood Cliffs, NJ: Prentice-Hall; 1999.
[21] Dullien AFL. Porous media: fluid transport and pore structure. 2nd ed. New York, NY: Academic Press; 1992.
[22] Taylor SC, Hall C, Hoff W, Wilson MA. Partial wetting in capillary liquid absorption by limestones. J Colloid Interface Sci 2000;224:351–7.
[23] Hall C. Water sorptivity of motars and concretes: a review. Mag Concr Res 1989;41:51–61.
[24] Miller EE. Similitude and scaling of soil–water phenomena. In: Hillel D, editor. Applications of soil physics. San Diego, California: Academic; 1980. p. 300–18.
[25] Youngs EC. Application of scaling to soil–water movement considering hysteresis. In: Hillel D, Elrich DE, editors. Scaling in soil physics: principles and applications, 25. SSSA Spec. Publ.; 1990. p. 23–7.
[26] Barry DA, Lisle IJ, Li L, Prommer H, Parlange J-Y, Sander GC, et al. Similitude applied to centrifugal scaling of unsaturated flow. Water Resour Res 2001;37(10):2471–9.
[27] Philip JR. The theory of infiltration, Part 4. Sorptivity and algebraic infiltration equations. Soil Sci 1957;84:257–64.
[28] Dunmore JM, Scholls RS. Drainage capillary pressure functions and the influence of connate water. SPE J 1974;14:437–44.

[29] Lenhard RJ, Parker JC. Measurement and prediction of saturation–pressure relationships in three-phase porous media systems. J Contam Hydrol 1987;1:407–24.
[30] Banno K. Centrifuge modeling of immiscible fingering in porous media. MS thesis, Massachusetts Institute of Technology, Cambridge MA, 1996.
[31] Culligan PJ, Banno K, Barry DA, Parlange J–Y. Preferential flow of a light non-aqueous phase liquid in dry sand. ASCE J Geotech Geoenviron Eng 2002;128(4):327–37.
[32] Lowry MI, Miller CT. Pore-scale modeling of nonwetting-phase residual in porous media. Water Resour Res 1995;31(3): 455–73.
[33] Bernadiner MG. A capillary microstructure of the wetting front. Transport Porous Med 1998;30:251–65.
[34] Toker NK, Germaine JT, Sjoblom KJ, Culligan PJ. A new technique for rapid measurement of continuous SMC curves. Geotechnique 2004;54(3):179–86.
[35] Ivanov VM. Measurements and interpretation of wetting infiltration in soils. Master of Science Thesis, Massachusetts Institute of Technology, Cambridge, MA, 2001.
[36] Steffy DA, Barry DA, Johnston CD. Improved scaling technique for two-phase pressure–saturation relationships. J Contam Hydrol 1997;28(3):207–25.
[37] Hassanizadeh SM, Celia MA, Dahle HK. Dynamic effect in the capillary pressure-saturation relationship and its impacts on unsaturated flow. Vadoze Zone J 2002;1:38–57.
[38] Bromwell LG. Friction of quartz in high vacuum. PhD thesis, Massachusetts Institute of Technology, Cambridge, MA, 1966.